Engineering Science & Technology
https://ojs.wiserpub.com/index.php/EST/

UNIVERSAL WISER PUBLISHER

Research Article

Activated Coconut Shell Charcoal Flakes as Supercapacitor Electrodes: Electrochemical Performance and Structural Characterization

R. R. M. M. N. B. Bambaradeniya[1], D. J. D. S. Gamage[1,2], A. P. S. P. Jayathilaka[1], A. D. T. Medagedara[1,2], H. A. M. M. Hapuarachchi[1], P. A. H. L. I. Pathiraja[1,3], K. Tennakone[1], R. M. G. Rajapakse[4], T. M. W. J. Bandara[2,5], G. R. A. Kumara[1*]

[1] National Institute of Fundamental Studies, Hantana Road, Kandy, 20000, Sri Lanka
[2] Postgraduate Institute of Science, University of Peradeniya, Peradeniya, 20400, Sri Lanka
[3] Department of Physics, Faculty of Science, University of Ruhuna, Matara, 81000, Sri Lanka
[4] Department of Chemistry, Faculty of Science, University of Peradeniya, Peradeniya, 20400, Sri Lanka
[5] Department of Physics, Faculty of Science, University of Peradeniya, Peradeniya, 20400, Sri Lanka
E-mail: kumara.as@nifs.ac.lk

Received: 14 July 2026; **Revised:** 14 August 2026; **Accepted:** 18 August 2026

Abstract: This study investigates the potential of utilizing coconut shell charcoal flakes as a sustainable precursor for Activated Carbon (AC) electrodes in supercapacitors. Five activation cycles labeled AC1 to AC5 were electrochemically and structurally analyzed using Raman spectroscopy, scanning electron microscopy, cyclic voltammetry, galvanostatic charge-discharge, electrochemical impedance spectroscopy, and long-term cycle stability testing methods. Raman spectra revealed distinct D and G bands near 1,345 cm^{-1} and 1,590 cm^{-1}. Among the samples, AC3 showed the most favorable structure, with an I_D/I_G ratio of 0.872, indicating a balanced degree of disorder and graphitic character that supported better electrochemical behavior. Microstructure analysis confirmed that AC3 possessed a well-developed, interconnected micropore-mesopore network, while over-activation in AC4 and AC5 led to pore merging and structural breakdown. Electrochemical results demonstrated that AC3 achieved the highest specific capacitance and energy density, reaching about 3.123 F g^{-1} and 0.434 W h kg^{-1} at a 10 mV s^{-1} scan rate. Impedance data showed that AC3 allowed effective ion transport and maintained a mainly capacitive response, with a moderate charge transfer resistance of around 6 Ω. In contrast, the over-activated samples exhibited reduced ion mobility. Long-term cycling tests confirmed that AC3 retained most of its capacitance after 1,000 charge-discharge cycles, indicating strong durability. Overall, coconut shell-based activated carbon, particularly at the AC3 activation stage, presents a cost-effective and eco-friendly electrode material with strong potential for advanced, sustainable supercapacitor applications.

***Keywords*:** supercapacitors, activated coconut shell charcoal flakes, physical activation

1. Introduction

The environmental concerns, high costs, and depletion of fossil fuels have shifted the interest of researchers in renewable energy sources like solar, wind, biomass, hydroelectricity, geothermal, and tidal energy [1]. The real challenge

Copyright ©2026 G. R. A. Kumara, et al.
DOI: https://doi.org/10.37256/est.81202710425
This is an open-access article distributed under a CC BY license
(Creative Commons Attribution 4.0 International License)
https://creativecommons.org/licenses/by/4.0/
*Some preliminary results of this work were presented as an abstract at the Postgraduate Institute of Science Research Congress (RESCON 2024) [30]. This manuscript adds new experiments and data, including Raman spectroscopy (I_D/I_G ratio) and Scanning Electron Microscopy (SEM) microstructural analysis, along with more in-depth analysis and discussion. The author list has also been expanded, with new authors making substantial contributions.

is not the scarcity of energy sources but harvesting energy efficiently from these sources and implementing efficient energy storage mechanisms. Herein, energy storage is important for facilitating easy access to energy and balancing the mismatch between energy generation and consumption periods [2]. While electrochemical batteries, fuel cells, and dielectric capacitors were historically the main electric energy storage devices, in recent decades, research has been focused on ultracapacitors, also known as supercapacitors, an intermediate system between electrochemical batteries, which store high energy with low power, and dielectric capacitors, which deliver high power within short bursts. Supercapacitors have lower energy densities and extremely higher-power densities than comparably sized batteries, and on the other hand, they have substantially larger energy densities and tend to have lower power densities than conventional capacitors [3]. Whilst the most notable feature of supercapacitors is their rapid charging-discharging capability, they possess other desirable features such as long cycle life and excellent capacity retention [4], [5]. These features make supercapacitors suitable for diverse applications such as transportation, defense, computing, medical, and industrial sectors [6].

Supercapacitors are classified into three main types: Electric Double-Layer Capacitors (EDLC), pseudo-capacitors, and hybrid supercapacitors. An EDLC consists of several parts, such as the electrode, the current collector, the electrolyte, the binder, and the separator, all of which affect the performance of the supercapacitor [3]. EDLC stores charge electrostatically like dielectric capacitors but with more storage due to the large surface area of the electrodes. By applying an external voltage between these electrodes, charges accumulate at the surface of the electrodes, which is balanced by the adsorption of oppositely charged ions from the electrolyte [3], [7]. This way, double layers of opposite charges are formed at the electrode-electrolyte interface. The electrode material must have high enough conductivity and a large surface area to form this double layer. In this regard, the surface area of the electrode is one of the major factors that determines the performance of an EDLC supercapacitor. The surface area of the electrode is based on the total surface area of the micropores, mesopores, and macropores. Cell capacitance is strongly correlated with the accessible surface area, provided that a hierarchical pore architecture exists to facilitate efficient ion transport to those active sites [8].

Biomass-derived porous carbons are widely used as electrode materials to fulfill this requirement, due to their large surface area, electrical conductivity, nontoxicity, abundance, low cost, and thermochemical stability [9]. Several bio-wastes, such as tea leaf residues, sugarcane bagasse, rice husk, nutshells, coconut shells, apricot shells, and neem, have been employed as precursor materials to obtain biomass-derived carbon. Among others, coconut shell-derived carbon is often preferred for supercapacitors due to its porous structure and high conductivity [10]. Coconut shell-derived carbons exhibit a unique amorphous structure with randomly oriented graphene layers. The hierarchical porous structure of coconut shell-derived carbon provides an interconnection between different pore-size structures and facilitates ion transport with minimal resistance [11], [12].

The surface area and porosity of coconut shell-derived carbon can be further improved through activation methods, mainly chemical and physical activations. Chemical activation involves agents like KOH, $ZnCl_2$, H_3PO_4, or NaOH, and physical activation is associated with high-temperature CO_2 treatment [13]-[15]. Out of them, physical activation is advantageous due to its cost-effectiveness and environmental friendliness. The two main stages of activating coconut shell-derived carbon are carbonization, where volatile compounds and hydrocarbons are removed from coconut shells at lower temperatures, and activation, which is done at high temperatures and yields a porous structure with a large surface area. Taken together, these steps produce an activated carbon material suitable for high-performance supercapacitor electrodes [16].

This study investigated the feasibility of utilizing activated coconut shell charcoal flakes directly as electrode materials for supercapacitors. A key objective of this work was to evaluate the practical advantage of employing intact flakes directly in situ rather than processing the material into a conventional powder. The structural and electrochemical properties of the resulting materials were systematically evaluated using Raman spectroscopy, scanning electron microscopy, cyclic voltammetry, galvanostatic charge-discharge analysis, electrochemical impedance spectroscopy, long-term cycle stability testing, and the assessment of capacitive-diffusive properties.

2. Materials and methodology

Coconut shells for producing activated carbon flakes were collected in coconut plantations located in the Kurunegala district of Sri Lanka. Titanium plates with dimensions of 20 mm × 10 mm × 0.45 mm (length × width × thickness) were used as the current collectors. Medium retention filter papers with a retention range of 10-13 µm (model-F1001) were obtained from Chemlab, Barcelona, Spain, and used as the separator. Sulfuric acid (H_2SO_4, 97%) and Ethanol (C_2H_6O, 99.9%) were acquired from Sigma-Aldrich, USA.

2.1 *The preparation of the AC and the supercapacitor cell*

The preparation of AC from coconut shells (Figure 1) involves several steps. First, cleaned coconut shells were subjected to low-oxygen carbonization by burning them in a closed container for 2 hours. Next, the charred shells were crumbled into flakes measuring approximately 1 cm × 1 cm, which were then thoroughly washed and dried on a hot plate overnight at 150 °C. After that, the flakes were put in a muffle furnace (Nabertherm-3,000, Germany) at 900 °C in a low-oxygen environment (tightly closed stainless steel container) for 20 minutes and subsequently quenched in a distilled water bath as previously described in a previous study. This process was repeated four times for the same sample. After each activation cycle, a small portion of the sample was taken. These fractions were designated as AC1, AC2, AC3, AC4, and AC5, indicating samples that had undergone exactly one, two, three, four, and five complete activation cycles, respectively.



Figure 1. Fabrication of supercapacitors utilizing AC

For supercapacitor cell assembly, the ACs were first trimmed and sanded to achieve uniform dimensions (4 mm × 4 mm × 1.5 mm) for each flake mass of 0.1 g. Next, the medium retention filter paper was placed between two prepared ACs. The assembly was positioned between the two titanium plates and clipped with a clamp. Finally, the separator was wetted with 2.5 M $H_2SO_{4(aq)}$ electrolyte to complete the supercapacitor cell preparation.

The microstructural morphology of prepared AC samples was examined using a ZEISS EVO-LS15 Scanning Electron Microscope (SEM) at different magnifications, with a constant tube voltage of 20 kV to obtain high-resolution

micrographs. Raman spectroscopy was conducted using a Renishaw Invia Reflex Raman spectrometer, recording the Raman shift with 514 nm excitation and spanning the wavenumber range of 500 cm^{-1} to 3,000 cm^{-1} for each AC sample.

The electrochemical performance of the fabricated supercapacitor cell was evaluated using Cyclic Voltammetry (CV), Galvanostatic Charge-Discharge (GCD), and Electrochemical Impedance Spectroscopy (EIS) with a two-electrode system utilizing an electrochemical workstation (Autolab, Netherlands).

The following equations were used to determine the cell-specific capacitance, energy density, power density, and the contribution of capacitive and diffusive control processes to the total current [17], [18].

$$C_s = \frac{Q}{2\nu m \Delta V} \tag{1}$$

$$E = \frac{C_s(\Delta V)^2}{2 \times 3.6} \tag{2}$$

$$P = \frac{3,600E}{\Delta t} \tag{3}$$

$$i(V) = k_1 \nu + k_2 \nu^{0.5} \tag{4}$$

The variables are defined as follows: C_s represents specific capacitance (F g^{-1}), Q denotes the charge obtained from the area under the CV curve in coulombs (C), ν is the scan rate (mV s^{-1}), m is the total mass of the active material in the electrode (g), and ΔV is the voltage range (V). The energy density (E) is expressed in (W h kg^{-1}), while the power density (P) is in (W kg^{-1}). The discharge time (Δt) is given in seconds (s). The constants k_1 and k_2 are associated with the capacitive and diffusive currents, respectively.

3. Results and discussion

3.1 *Structural analysis*

Raman spectra for cells AC1 to AC5 are shown in Figure 2, with distinct peaks around 1,345 cm^{-1} and 1,590 cm^{-1}, corresponding to the D-band and G-band, respectively. These bands are typical for carbon-based materials [19]. G-band indicates the presence of graphitic domains within the material, reflecting the ordered nature of carbon structures. D-band is associated with the presence of structural defects and disordered carbon within the material, reflecting the amorphous and porous nature of carbon materials.

As the activation cycle progresses from AC1 to AC5, an increase in the intensity of both the D-band and G-band peaks can be observed. This increase in intensities of the D-band and G-band with each activation cycle suggests that the samples undergo structural transformations, enhancing both defect sites and graphitic domains.

The ratio of the intensities of the D-band to the G-band (I_D/I_G) was calculated to evaluate the degree of disorder in the samples. An increase in the I_D/I_G ratio suggests a higher degree of amorphous carbon content, whereas a lower ratio indicates a more ordered, graphitic structure. The I_D/I_G ratio in Table 1 exhibits relative stability with minor fluctuations among samples, with AC3 demonstrating a greater level of disorder.

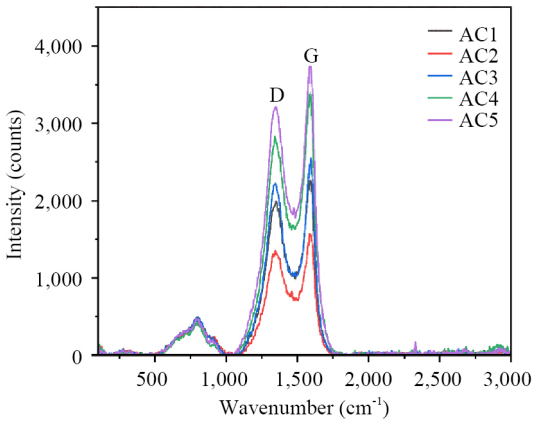


Figure 2. Raman spectra of each AC sample

Table 1. The table of I_D/I_G ratio calculated from the Raman spectra

Sample	I_D (cm^{-1})	I_G (cm^{-1})	I_D/I_G
AC1	1,191	1,763	0.675
AC2	1,311	1,575	0.832
AC3	2,218	2,544	0.872
AC4	2,826	3,393	0.833
AC5	3,208	3,738	0.858

SEM images of samples in Figure 3 (AC1 to AC5) reveal progressive morphological changes induced by the activation process. The carbonized sample displays a dense, compact structure with a smooth surface and minimal porosity, indicating that initial carbonization mainly removes volatiles without developing significant pore structures. With the AC1, small, shallow pores begin to emerge across the surface. Although limited in depth and interconnectivity, this early-stage porosity slightly increases the surface area. In AC2, the porous structure becomes more pronounced, with increased micropore formation and the emergence of mesopores. AC3 exhibits a well-developed, hierarchical porous network characterized by a uniform distribution of interconnected micro- and mesopores. This optimal balance enhances both the surface area for charge storage and the pathways for efficient ion diffusion, key factors contributing to AC3's highest observed capacitance. The interconnected pores facilitate rapid ion transport, reducing internal resistance during charge-discharge cycles [20]. In AC4, the porous network expands further with the appearance of larger mesopores and early-stage macropores. However, this comes at the cost of reduced micropore density. While larger pores can improve ion transport, the decline in micropores, critical for high surface area, diminishes charge storage capacity, leading to reduced capacitance. By AC5, over-activation results in extensive mesopore and macropore development, with thinning pore walls and less defined structures. The continued loss of microporosity and structural integrity causes a decline in effective surface area. This excessive pore enlargement compromises the electrode's performance by reducing the number of active sites for ion adsorption. Overall, AC3 represents the optimal activation level, offering a balanced pore architecture that maximizes both ion-accessibility and surface area. Beyond this point, further activation leads to structural degradation and a reduction in electrochemical performance.

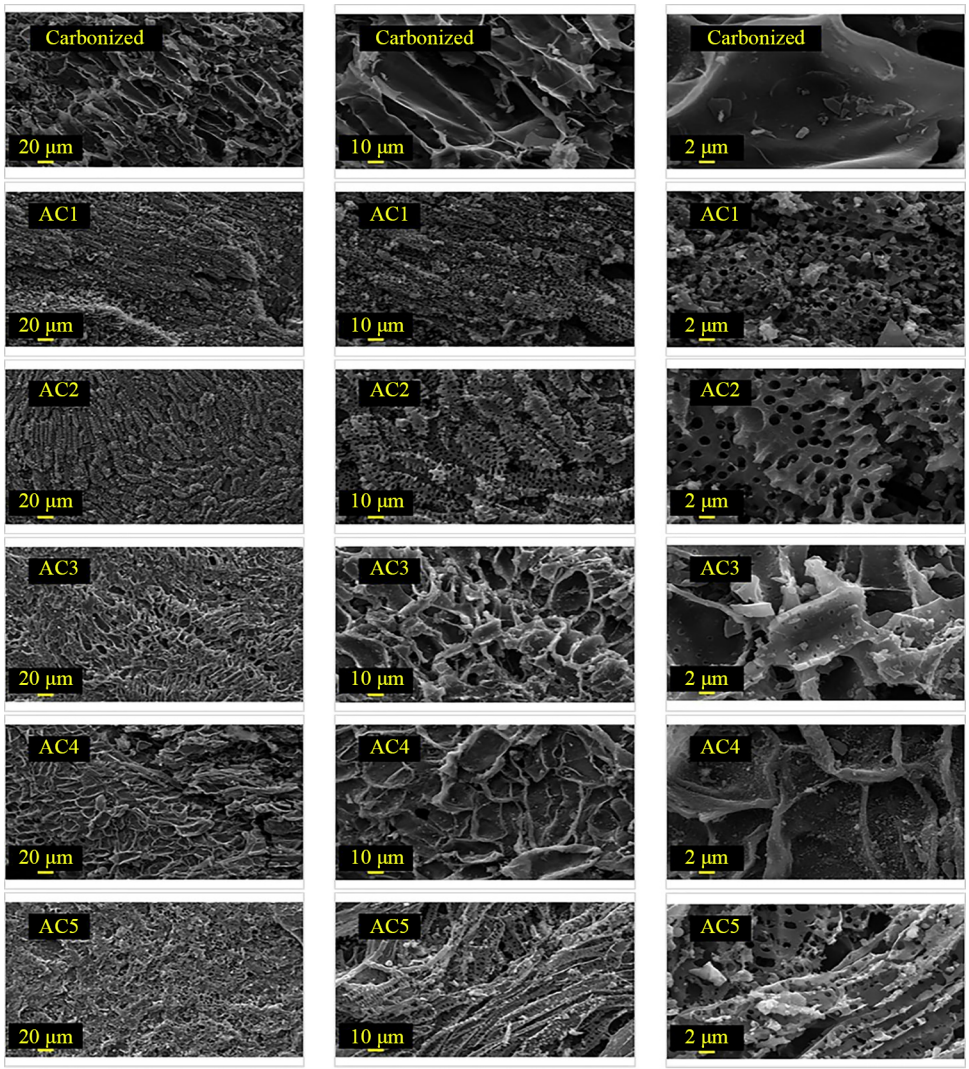


Figure 3. SEM images of carbonized and AC samples at magnifications of × 500, × 1,500, and × 5,000

3.2 *Electrochemical characterization*

Table 2. Comparison of recent literature on activated carbon-based electrodes in two-electrode supercapacitor systems

Electrode material	Electrode setup	Electrolyte	C_s (F g^{-1})	Reference
AC	Two electrode system	1 M Tetraethylammonium tetrafluoroborate ($TEABF_4$)	26	[21]
AC		1 M NaCl	30–36	[22]
AC		2.5 M H_2SO_4	74.35	[23]
AC		6 M KOH	85–90	[24]
Porous carbon		6 M KOH	143	[25]
Activated coconut shell flakes		2.5 M H_2SO_4	3.1	This work

The CV curves of samples AC1 to AC5 exhibit the typical EDLC behavior of supercapacitor materials. At low scan rates (5-10 mV s^{-1}), all samples display near-rectangular and symmetrical shapes, indicating efficient ion adsorption at

the electrode-electrolyte interface and rapid charge-discharge kinetics. The absence of redox peaks across all scan rates confirms the dominance of non-faradaic EDLC behavior.

Table 2 compares the specific capacitance of various carbon-based electrode materials across different electrolytes in two-electrode systems. The data illustrates that electrochemical performance is highly dependent on the chosen electrolyte and carbon morphology, highlighting the influence of these parameters on overall charge storage capacity.

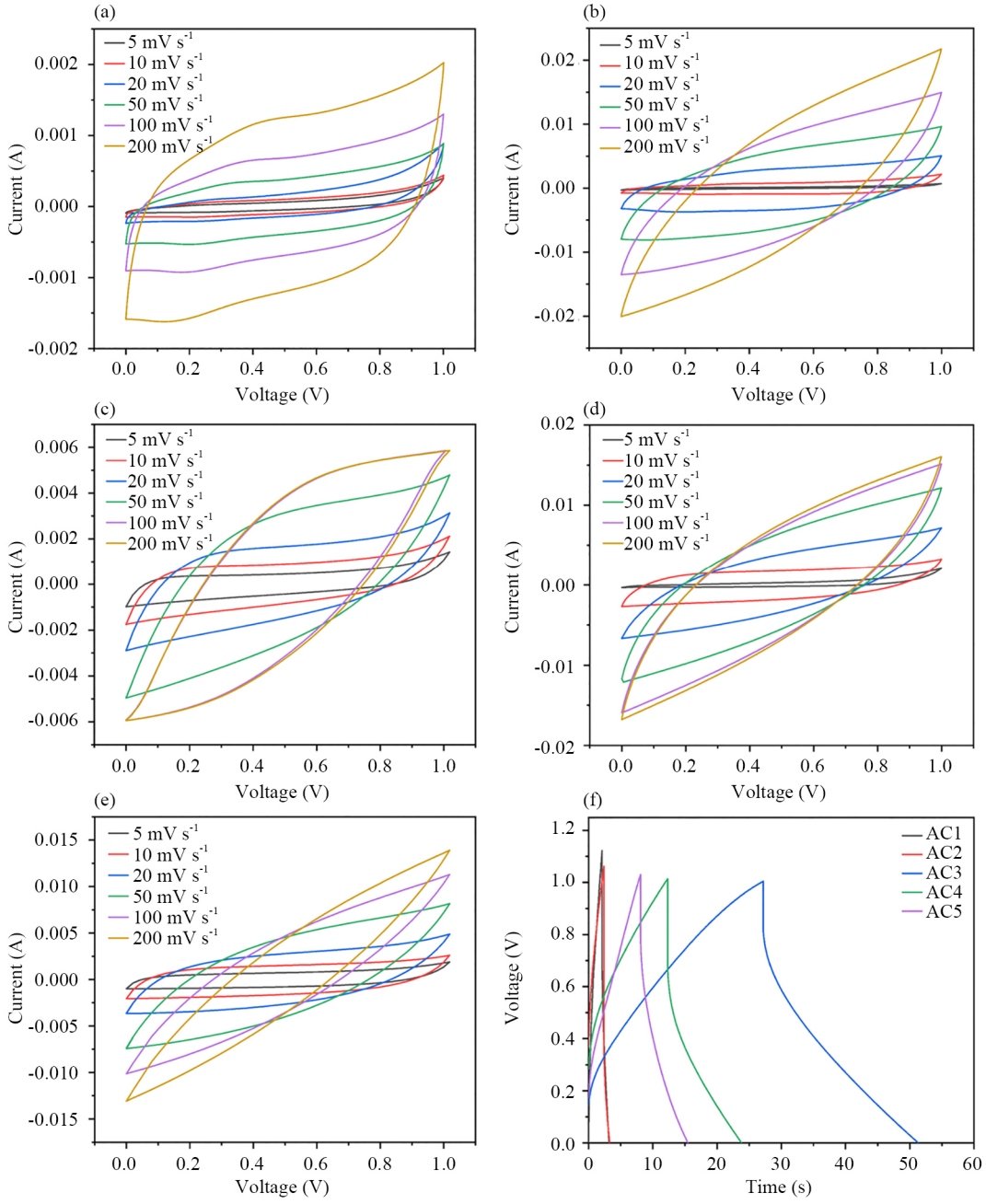


Figure 4. CV graphs with varying scan rates for each sample (a) AC1, (b) AC2, (c) AC3, (d) AC4, (e) AC5, and (f) GCD at 0.1 A g^{-1} for all samples

In Figure 4a to Figure 4e, as scan rates increase (up to 200 mV s^{-1}), deviations from the ideal rectangular shape are observed, particularly in AC4 and AC5. These distortions reflect limitations in ion diffusion at higher rates and a reduction

in accessible surface area. From AC1 to AC3, the CV curves show progressively larger areas under the curve at each scan rate, signifying improved capacitance. This enhancement correlates with increased surface area and porosity observed in SEM and Raman analyses, suggesting that moderate activation effectively optimizes the electrode structure. In contrast, AC4 and AC5 display diminished current response and slight distortions in CV shape, particularly at higher scan rates. This performance decline is attributed to over-activation, which leads to excessive pore enlargement and coalescence, reducing micropore density and thereby the effective surface area for charge storage. Overall, CV analysis confirms that AC3 achieves the optimal balance between micropores and mesopores, maximizing both ion accessibility and charge storage capability. Beyond this point, structural degradation due to over-activation adversely affects electrochemical performance.

GCD curves of samples AC1 to AC5, Figure 4f, recorded at a current density of 0.1 A g^{-1}, provide insights into the charge-discharge characteristics of the AC electrodes. AC1 displays a relatively short charge-discharge duration, indicating low capacitance due to limited activation and surface area.

In AC2, the discharge time increases, reflecting improved capacitance, attributed to enhanced surface area and pore accessibility from further activation. AC3 exhibits the longest discharge duration among all samples, signifying the highest specific capacitance. This suggests that AC3 achieves an optimal balance of micropores and mesopores, maximizing ion-accessible surface area and promoting efficient charge storage.

In contrast, AC4 shows a reduction in discharge time compared to AC3. This decline results from over-activation, where the coalescence of smaller pores into larger ones reduces the effective surface area. AC5 continues this trend, with an even shorter discharge time, confirming a further loss in capacitance due to structural degradation. A voltage drop is observed at the beginning of each discharge curve across all samples, indicative of the internal Equivalent Series Resistance within the cells [26]. Overall, the GCD results in Tables 3 and 4 support the conclusion that AC3 provides the optimal activation level for supercapacitor performance. Beyond this point, excessive activation leads to diminished charge storage capacity due to pore widening and structural inefficiencies [27].

Table 3. The C_s and E at different scan rates for each AC sample

Scan rate (mV s^{-1})	AC1		AC2		AC3		AC4		AC5	
	C_s	E	C_s	E	C_s	E	C_s	E	C_s	E
5	0.326	0.0453	1.022	0.1420	2.801	0.3890	2.527	0.3509	2.726	0.3786
10	0.293	0.0407	2.259	0.3138	3.123	0.4338	3.072	0.4266	2.986	0.4147
20	0.356	0.0495	2.878	0.3997	3.060	0.4249	3.040	0.4223	2.261	0.3140
50	0.251	0.0349	2.102	0.2919	2.226	0.3091	2.118	0.2941	1.389	0.1930
100	0.168	0.0233	1.260	0.1751	1.284	0.1784	1.072	0.1488	0.847	0.1177
200	0.132	0.0184	0.730	0.1014	0.750	0.1041	0.677	0.0940	0.397	0.0552

Table 4. The power density calculation for the fabricated cell at a current density of 0.1 A g^{-1}

Current density (A g^{-1})	Power densities of AC samples (W kg^{-1})				
	AC1	AC2	AC3	AC4	AC5
0.1	46.652	27.062	138.058	52.137	86.311

EIS measurements (Figure 5) were performed to evaluate the charge-transfer resistance, ion diffusion, and overall electrochemical behavior of the electrodes AC1 through AC5 [28]. Samples AC1 and AC2 display relatively small semicircles accompanied by shallow low-frequency tails. This profile indicates limited ion diffusion and poor capacitive performance. Sample AC4 exhibits a smaller semicircle diameter relative to AC3 alongside a less steep tail, suggesting a

decline in ion transport efficiency caused by pore overexpansion. Sample AC5 shows further deterioration with a flatter tail and reduced capacitive behavior resulting from excessive activation and compromised pore architecture.

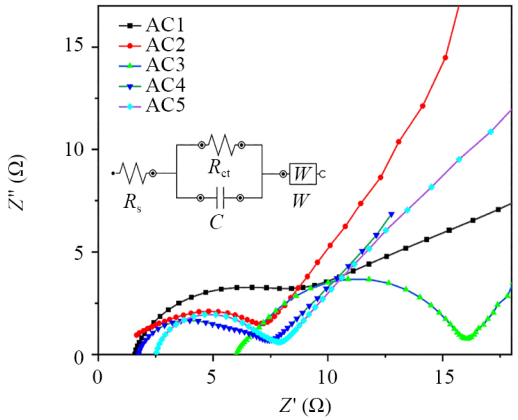


Figure 5. EIS plot for each AC sample

Sample AC3 exhibits a more pronounced semicircle. The impedance data for the AC3 cell were fitted to a Randles equivalent circuit model to quantify the electrochemical parameters. The fitting yields an equivalent series resistance (R_s) of 2.22 Ω and a charge transfer resistance (R_{ct}) of 4.70 Ω. The circuit model also identifies a parallel capacitance (C) of 13.5 μF and a Warburg impedance of 75.6 mMho s^{-1}. Despite having a higher R_{ct} than in the initial activation stages, AC3 exhibits a steep, near-vertical low-frequency tail. This feature reflects superior ion diffusion and strong capacitive behavior.

While the charge transfer resistance provides valuable insight into the electrode-electrolyte interface, the low-frequency region remains equally critical for assessing electrode efficacy [29]. The optimized pore structure of AC3 supports enhanced ion transport. This configuration demonstrates the most favorable balance of pore architecture and electrochemical characteristics among all the evaluated samples.

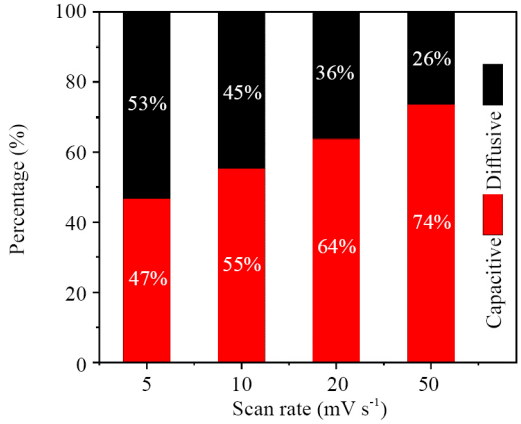


Figure 6. Contribution of capacitive and diffusive control processes to the total current in the AC3 cell

The capacitive and diffusive properties analysis and the cyclic stability test were performed only for the AC3 sample to use resources efficiently and to focus on the most promising cell. This is because the Raman, SEM, CV, GCD analysis, and EIS collectively indicated that AC3 exhibited the optimal balance of electrochemical performance, surface area, and

pore structure. Unlike AC1 and AC2, which showed limited pore development, and AC4 and AC5, where excessive activation led to pore coalescence and a decrease in effective surface area, AC3 maintained a well-defined porous structure associated with efficient ion diffusion.

CV curves for the AC3 cell were further analyzed to determine the cell contribution of capacitive and diffusive control processes to current density. As in Figure 6, results show that capacitive contribution increases with scan rate. At 5 mV s^{-1}, the capacitive and diffusive contributions are 47% and 53%, respectively. At 200 mV s^{-1}, the capacitive share rises to 74%, while the diffusive component drops to 26%.

This trend indicates that at low scan rates, ions have sufficient time to diffuse into the deeper pores of the electrode, enhancing the diffusion-controlled process [23]. Conversely, at higher scan rates, ion access is largely limited to surface or near-surface regions, favoring capacitive storage. The increasing capacitive dominance at elevated scan rates confirms that the AC3 sample possesses a well-developed porous structure conducive to rapid ion transport and efficient surface-based charge storage.

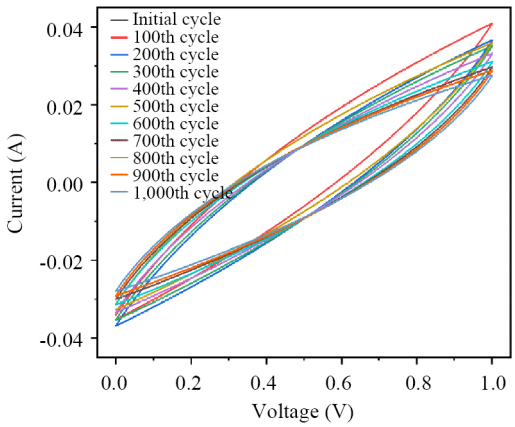


Figure 7. The cyclic stability test for the AC3 cell was conducted using the CV technique at a scan rate of 200 mV s^{-1} over 1,000 cycles

The cyclic stability data provide an initial assessment of the electrochemical durability of the activated carbon electrode material over 1,000 cycles. The voltammograms (Figure 7) maintained a consistent, near-rectangular shape from the initial sweep to the final cycle, which indicates a stable retention of capacitive behavior. Furthermore, the minimal variation in current response between the 100th and 1,000th cycles suggests high coulombic efficiency and consistent energy retention within this testing window. While this stability highlights the structural integrity of the activated carbon matrix under preliminary electrical stress, extended continuous cycling is required to fully confirm its viability for long-term operations. Ultimately, the direct utilization of binder-free coconut shell flakes presents a viable methodology for fabricating electrodes suited for small-scale energy storage applications.

4. Conclusion

This study demonstrates the feasibility of using intact coconut shell charcoal flakes as a sustainable, binder-free material for activated carbon electrodes. The sequential physical activation process successfully developed a porous architecture within the charcoal. Among the evaluated samples under the specific experimental conditions, the AC3 cell exhibited the best performance by achieving an optimal balance of pore structure and electrochemical properties. Characterization results confirmed that excessive activation beyond the AC3 stage leads to structural collapse and diminished performance due to pore coalescence. The AC3 electrode displayed reliable electrochemical stability over 1,000 charge and discharge cycles. We acknowledge the operational limitations of this study. The specific capacitance remains modest compared to optimized powder systems due to the dense macro-scale nature of the flakes. The absence

of quantitative porosity data also requires future investigation. These results establish the foundational potential of direct-flake activated carbon as a cost-effective approach for sustainable electrode fabrication.

Declaration of generative AI technologies

During the preparation of this manuscript, the authors used Gemini Pro (Google) solely for the purposes of language editing, stylistic improvements, and reference list formatting. Following the use of this tool, the authors reviewed and edited the material to ensure scientific accuracy, and they take full responsibility for the entirety of the published article.

Author contributions

R. R. M. M. N. B. Bambaradeniya: Writing—original draft, Validation, Methodology, Investigation, Formal analysis, Data curation. D. J. D. S. Gamage: Writing—original draft, Validation, Investigation, Formal analysis, Data curation. A. P. S. P. Jayathilaka: Writing—original draft, Formal analysis, Data curation. A. D. T. Medagedara: Validation, Methodology, Investigation, Data curation. H. A. M. M. Hapuarachchi: Methodology, Formal analysis. P. A. H. L. I. Pathiraja: Methodology, Formal analysis. K. Tennakone: Writing—review & editing, Visualization, Validation. R. M. G. Rajapakse: Writing—review & editing, Visualization, Validation. T. M. W. J. Bandara: Writing—review & editing, Validation. G. R. A. Kumara: Writing—review & editing, Visualization, Validation, Supervision, Project administration, Conceptualization. All authors reviewed and approved the final manuscript and agreed to be accountable for the work.

Funding

This research received no external funding.

Data availability

All data supporting the findings of this study are presented within the article. Additional data may be made available by the corresponding author upon reasonable request.

Conflict of interest

The authors declare that they have no known competing financial interests or personal relationships that could have appeared to influence the work reported in this paper.

References

[1] A. Stancu, C. Popescu, M. Panait, I. G. Rădulescu, A. G. Brezoi, and M. C. Voica, "Pathways to carbon neutrality: Innovations in climate action and sustainable energy," *Sustainability*, vol. 17, no. 24, p. 11240, 2025.

[2] A. T. Admase, E. D. Asrade, and S. W. Fanta, "A comprehensive review on energy storage materials & technologies: Applications of nanofabrication techniques for enhanced performance and efficiency," *Materials for Renewable and Sustainable Energy*, vol. 14, no. 3, p. 56, 2025.

[3] L. Pinoski, S. A. Jose, J. Dowling, N. Eastwood, C. Farthing, G. Fisher, et al., "Supercapacitor materials: Structure, properties, and applications for energy storage in engineering systems," *Materials*, vol. 19, no. 12, p. 2454, 2026.

[4] K. Li, P. Li, Z. Sun, J. Shi, M. Huang, J. Chen, et al., "All-cellulose-based quasi-solid-state supercapacitor with nitrogen and boron dual-doped carbon electrodes exhibiting high energy density and excellent cyclic stability," *Green Energy & Environment*, vol. 8, no. 4, pp. 1091-1101, 2023.

[5] M. Czagany, S. Hompoth, A. K. Keshri, N. Pandit, I. Galambos, Z. Gacsi, et al., "Supercapacitors: An efficient way for energy storage application," *Materials*, vol. 17, no. 3, p. 702, 2024.

[6] J. R. Miller and A. Burke, "Electrochemical capacitors: Challenges and opportunities for real-world applications," *The Electrochemical Society Interface*, vol. 17, no. 1, pp. 53-57, 2008.

[7] P. Simon and Y. Gogotsi, "Charge storage mechanism in nanoporous carbons and its consequence for electrical double layer capacitors," *Philosophical Transactions of the Royal Society A: Mathematical, Physical and Engineering Sciences*, vol. 368, no. 1923, pp. 3457-3467, 2010.

[8] Y. Li, H. Shen, Y. Zhu, I. Zada, F. Song, Q. Liu, et al., "Hierarchical pore engineering of lignocellulose-based carbon materials for electric double-layer capacitors," *Nano Research*, vol. 18, no. 10, p. 94907960, 2025.

[9] J. Deng, M. Li, and Y. Wang, "Biomass-derived carbon: Synthesis and applications in energy storage and conversion," *Green Chemistry*, vol. 18, no. 18, pp. 4824-4854, 2016.

[10] L. Lyu, K. Seong, D. Ko, J. Choi, C. Lee, T. Hwang, et al., "Recent development of biomass-derived carbons and composites as electrode materials for supercapacitors," *Materials Chemistry Frontiers*, vol. 3, no. 12, pp. 2543-2570, 2019.

[11] M. B. Idris, B. B. Mamba, and F. Xolile, "Hierarchical pore engineering in waste-derived carbons for supercapacitors: Bridging the performance gap from three-electrode evaluation to practical two-electrode devices," *RSC Advances*, vol. 16, no. 32, pp. 29368-29398, 2026.

[12] Y. Wang, Y. Duan, X. Liang, L. Tang, L. Sun, R. Wang, et al., "Hierarchical porous activated carbon derived from coconut shell for ultrahigh-performance supercapacitors," *Molecules*, vol. 28, no. 20, p. 7187, 2023.

[13] M. K. B. Gratuito, T. Panyathanmaporn, R. A. Chumnanklang, N. Sirinuntawittaya, and A. Dutta, "Production of activated carbon from coconut shell: Optimization using response surface methodology," *Bioresource Technology*, vol. 99, no. 11, pp. 4887-4895, 2008.

[14] N. M. Keppetipola, M. Dissanayake, P. Dissanayake, B. Karunarathne, M. A. Dourges, D. Talaga, et al., "Graphite-type activated carbon from coconut shell: A natural source for eco-friendly non-volatile storage devices," *RSC Advances*, vol. 11, no. 5, pp. 2854-2865, 2021.

[15] M. Amin, E. Chung, and H. H. Shah, "Effect of different activation agents for activated carbon preparation through characterization and life cycle assessment," *International Journal of Environmental Science and Technology*, vol. 20, no. 7, pp. 7645-7656, 2023.

[16] M. Galinski, K. Babeł, and K. Jurewicz, "Performance of an electrochemical double layer capacitor based on coconut shell active material and ionic liquid as an electrolyte," *Journal of Power Sources*, vol. 228, pp. 83-88, 2013.

[17] S. Sharma and P. Chand, "Supercapacitor and electrochemical techniques: A brief review," *Results in Chemistry*, vol. 5, no. 1, p. 100885, 2023.

[18] J. Wang, J. Polleux, J. Lim, and B. Dunn, "Pseudocapacitive contributions to electrochemical energy storage in TiO_2 (anatase) nanoparticles," *The Journal of Physical Chemistry C*, vol. 111, no. 40, pp. 14925-14931, 2007.

[19] A. Sadezky, H. Muckenhuber, H. Grothe, R. Niessner, and U. Pöschl, "Raman microspectroscopy of soot and related carbonaceous materials: Spectral analysis and structural information," *Carbon*, vol. 43, no. 8, pp. 1731-1742, 2005.

[20] Y. Zhang, R. Ma, B. Zhang, D. Jia, L. Wang, and N. Guo, "Long/short-range ordered porous carbon with interconnected structure for high performance supercapacitor," *Journal of Energy Storage*, vol. 94, p. 112531, 2024.

[21] P. Ruschhaupt, A. Varzi, and S. Passerini, "Natural polymers as green binders for high-loading supercapacitor electrodes," *Chemistry-Sustainability-Energy-Materials*, vol. 13, no. 4, pp. 763-770, 2020.

[22] G. Landi, L. La Notte, A. L. Palma, A. Sorrentino, M. G. Maglione, and G. Puglisi, "A comparative evaluation of sustainable binders for environmentally friendly carbon-based supercapacitors," *Nanomaterials*, vol. 12, no. 1, p. 46, 2021.

[23] P. M. Kumarage, D. S. Gamage, A. T. Medagedara, M. I. U. Weerasinghe, S. P. Jayathilaka, A. M. Rathnayake, et al., "Pyrolyzed sucrose as a green binder for coconut shell-based activated carbon electrodes in supercapacitors," *Applied Nano*, vol. 7, no. 3, p. 19, 2026.

[24] R. K. Azega, M. M. Haque, A. Vyas, P. L. Tam, A. D. Smith, P. Lundgren, et al., "Durable activated carbon electrodes with a green binder," *Physica Status Solidi B: Basic Solid State Physics*, vol. 259, no. 2, p. 2100311, 2022.

[25] M. Skorupska, P. Kamedulski, J. P. Lukaszewicz, and A. Ilnicka, "The improvement of energy storage performance by sucrose-derived carbon foams via incorporating nitrogen atoms," *Nanomaterials*, vol. 11, no. 3, p. 760, 2021.
[26] J. Zhao and A. F. Burke, "Electrochemical capacitors: Performance metrics and evaluation by testing and analysis," *Advanced Energy Materials*, vol. 11, no. 1, p. 2002192, 2021.
[27] S. Li, X. Tan, H. Li, Y. Gao, Q. Wang, G. Li, et al., "Investigation on pore structure regulation of activated carbon derived from sargassum and its application in supercapacitor," *Scientific Reports*, vol. 12, no. 1, p. 10106, 2022.
[28] Y. P. Hardianto, S. S. Shah, M. M. Mohamed, S. Sarker, and Md. A. Aziz, "Fundamentals of electrochemical impedance spectroscopy in energy storage devices: Principles and innovative curve fitting approaches," *Discover Electronics*, vol. 3, no. 1, p. 9, 2026.
[29] J. D. George, W. Brenneis, V. K. Sangwan, D. Meli, H. Kurtz, J. Richards, et al., "Robust interpretation of electrochemical impedance spectra using numerical complex analysis," *ACS Measurement Science Au*, vol. 6, no. 2, pp. 324-339, 2026.
[30] R. R. M. M. N. B. Bambaradeniya, A. P. S. P. Jayathilaka, A. D. T. Medagedara, and G. R. A. Kumara, "Feasibility of coconut shell flakes derived activated carbon electrodes for supercapacitors," in Proceedings of RESCON, 2024, p. 193.